Electronic Supplementary Information For

Quantitative Analysis of Weak Current Rectification in Molecular Tunnel Junctions Subject to Mechanical Deformation Reveals Two Different Rectification Mechanisms for Oligophenylene Thiols versus Alkane Thiols

Zuoti Xie,[†,‡,*,#] Ioan Bâldea,[§,*,#] Quyen Van Nguyen,[‡] and C. Daniel Frisbie[‡,*]

[†]*Department of Materials Science and Engineering, Guangdong Technion-Israel Institute of Technology, Shantou, Guangdong, 515063, China*
[‡]*Department of Chemical Engineering and Materials Science, University of Minnesota, Minneapolis, Minnesota, 55455, United States*
[§]*Theoretical Chemistry, Heidelberg University, INF 229, D-69120 Heidelberg, Germany*
[#] Equal contribution
*To whom correspondence should be addressed:
E-mail: zuoti.xie@gtiit.edu.cn; ioan.baldea@pci.uni-heidelberg.de; frisbie@umn.edu

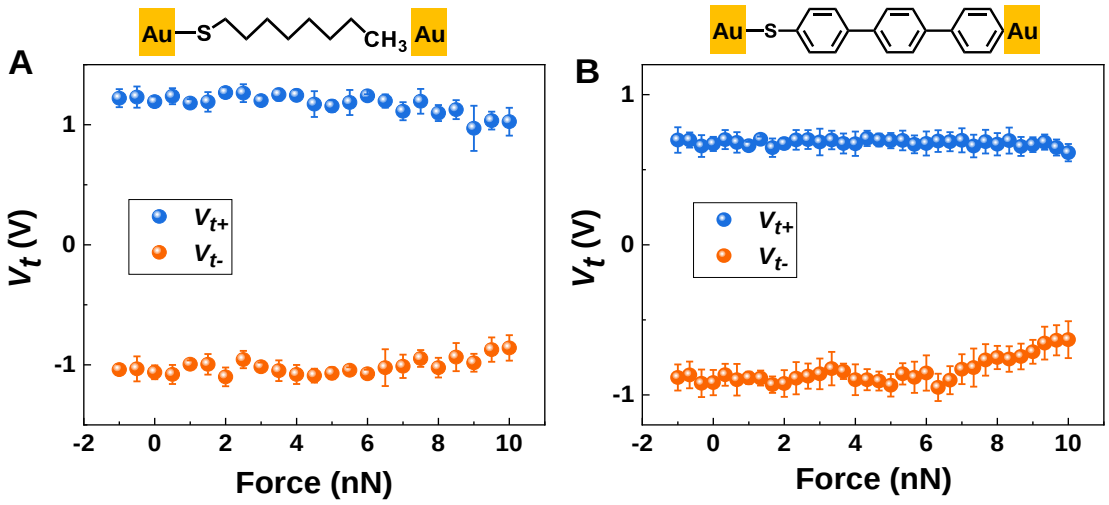

Figure S1. Impact of mechanical stretching on the transition voltages of CnT and OPTn junctions with gold electrodes.

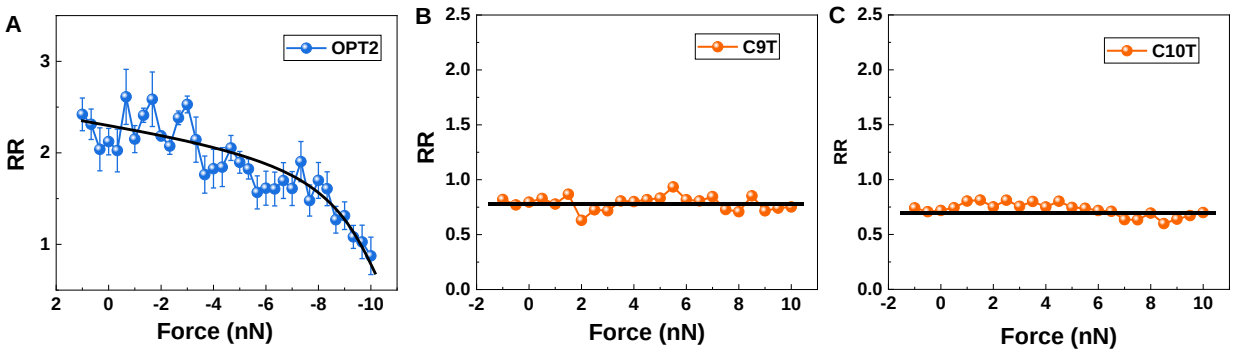

Figure S2. Current rectification ratio (RR) for OPT2, C9T, and C10 T junctions as a function of the mechanical stretching force F.

Demonstration that RR(V→0) =1 Holds for Any Transport Mechanism By Tunneling

To see that charge transport by tunneling in two-terminal setup can yield current rectification only at sufficiently large biases, one can start from the general trace formula[1,2]:

$$\mathrm{I(V)} = \frac{2e}{h}\int d\varepsilon[f\left(\varepsilon - \frac{eV}{2}, T_L\right) - f(\varepsilon + \frac{eV}{2}, T_R)]\zeta(\varepsilon; V, \dots)$$

$$\equiv \mathrm{I(V, \dots)} \qquad \text{(S1)}$$

where the two functions $f(\varepsilon \mp eV/2\,, T_{L,R})$ stand for the Fermi electronic distributions of the "left"(L) and "right" (R) electrodes at temperatures $T_{L,R}$.

The RHS of the above equation is a general function $\mathrm{I(V, \dots)}$ of bias (V) and other properties (denoted here by "…" and omitted below for the sake of simplicity of the embedded molecules (e. g., MO energies), electrodes (e.g., Fermi energy, DOS) and their couplings (often denoted by Γ). It can be expressed as a (Talor) power series expansion in V:

$$\mathrm{I(V)} = \mathrm{GV} + G_2V^2 + G_3V^3 + \vartheta(V^4) \qquad \text{(S2)}$$

Notice that, save for situations (e.g., thermopower measurements) wherein temperature gradients are applied, the electrode temperatures are equal $T_L = T_R = T$, which makes the zero order term (V^0) in the above formula vanish. Eq S2 straightforwardly yields:

$$\mathrm{RR(V)} \equiv -\frac{I(V)}{I(-V)} = 1 + \frac{2G_2}{G}V + \frac{2G_2^2}{G^2}V^2 + \frac{2G_2(G_2^2 - GG_3)}{G^3}V^3 + \vartheta(V^4) \qquad \text{(S3)}$$

which shows that

$$\mathrm{RR(V)}|_{V=0} \equiv 1 \qquad \text{(S4)}$$

As noted in the main text; tunneling mechanisms can yield current rectification RR $\neq 1$ only at sufficiently large biases where the $\mathrm{I}-\mathrm{V}$ curves are not only nonlinear but also asymmetric upon bias polarity reversal ($G_2 \neq 0$).

Notations and Some Useful Relations

For reader's benefit, we present here a summary of several symbols used in this paper that might create confusion:

$V \equiv V_{junction} = V_t - V_s$: experimentally relevant ("external") bias applied to the junction, representing the difference between tip's and substrate's potentials V_t and V_s, respectively.

$V_{vac}(z)$: unscreened potential, representing a linear interpolation between substrate's and tip's potentials: $V_{vac}(z_{s,t}) = Vs,t$. Its derivative with reversed sign represents the external (unscreened) field $E_{ext} \equiv E_z = -dV_{vac}(z)/dz$ whose value is an input parameter in quantum chemical calculations.

$v(\mathbf{r}) \equiv v(x,y,z)$: internal, microscopic potential (embodying intramolecular screening) obtained in this paper via quantum chemical calculations considering an external (unscreened) bias V between the molecule's ends. We should have written $v(\mathbf{r}; V) \equiv v(x,y,z; V)$ but have skipped the argument V to avoid a too complicated notation. The same applies to the next two symbols, for which a more complete/rigorous notation, $v(z; V)$ and $\bar{v}(z; V)$, should have been used.

$v(z)$: internal, microscopic potential (embodying intramolecular screening) along Oz axis connecting the S and C atoms at molecule's ends computed by averaging the microscopic potential over the (x, y) transverse directions weigthed by HOMO's spatial distribution; it is a HOMO-dedicated property (see eq (S12)).

$\bar{v}(z)$: coarse grain average of the microscopic potential *v(z)* whose linear dependence on *z* is obtained by fitting the curve of *v(z)* extracted from quantum chemical calculations. Its derivative with reversed sign represents the internal (screened) field $E_{internal} = -d\bar{v}(z)/dz$. Its strict proportionality to E_{ext} backed by extensive quantum calculations allows to define a dielectric constant

$$\kappa \equiv \frac{E_{ext}}{E_{internal}} \qquad \text{(S5)}$$

which turns out to be an important molecular property for the analysis presented in this paper.

$V_{molec} = \bar{v}(z_t) - \bar{v}(z_s)$: bias at molecular ends responsible for the HOMO energy shift. The relationship

$$V_{molec} = \frac{V_{junction}}{\kappa} = \frac{V}{\kappa} \qquad \text{(S6)}$$

is the direct consequence of eq (S5). Notice that this κ is a HOMO-dedicated property of the molecule and should by no means be confused with the macroscopic SAM's dielectric function. For the reader less acquainted with the notion of (HO)MO's center of charge, whose longitudinal coordinate

$$z_{HOMO} \equiv \langle z \rangle = \frac{\int z\, \rho_{HOMO}(x,y,z)dxdydz}{\int \rho_{HOMO}(x,y,z)dxdydz} = \int z\, \rho_{HOMO}(z)dz$$

defined by eq (7) in the main text and repeated here for the reader's convenience, we refer here to the more familiar center of mass (CM). For a collection of discrete points having masses m_1, m_2, m_3, ... located at $\mathbf{r}_1$, $\mathbf{r}_2$, $\mathbf{r}_3$, ..., the CM position is defined by $\boldsymbol{r}_{CM} = \frac{\sum_j m_j \boldsymbol{r}_j}{\sum_j m_j}$. For a continuum mass distribution characterized by a mass density ρ(**r**) at point **r**, the above expression yields

$$\boldsymbol{r}_{CM} = \frac{\int \boldsymbol{r}\, \rho(\boldsymbol{r})\, d\boldsymbol{r}}{\int \rho(\boldsymbol{r})\, d\boldsymbol{r}}$$

Noting that the (HO)MO spatial density is normalized – i.e., $\int \rho(\boldsymbol{r})\, d\boldsymbol{r} = 1$–, the above formula is nothing but the counterpart of eq (7) of the main text.

To end this section we note that, in order to keep notation reasonably simple, in the various formulas and figures presented across this paper we implicitly assume that the coordinates of the atoms S and C at the ends of the OPT3 molecule and the location of substrate and tip interfaces do not notably differ ($z_S \approx z_s$ and $z_C \approx z_t$, respectively).

Derivation of Several Important Forumulas Related to the Potentiometric Rule Utilized in the Main Text

Assuming (cf. Figure S3) a vacuum-like potential profile $V_{vac}(z)$ varying linearly across a junction along Oz axis between the values $-V/2$ and $+V/2$ at the electrode locations at z_s and z_t, ($z_s < z_t$) respectively yields the following expression

$$V_{vac}(z) = \frac{V}{z_t - z_s}(z - z_0) \qquad \text{(S7)}$$

where

$$z_0 \equiv \frac{z_s + z_t}{2} \qquad \text{(S8)}$$

For a point-like HOMO (to refer to the specific case under present consideration) located at z_{HOMO}, eq (S5) yields a bias dependent energy of the form

$$\varepsilon_0(V) \equiv -\varepsilon_h + \delta\varepsilon_0(V) = -\varepsilon_h - eV(z) = -\varepsilon_h - eV\frac{z_{HOMO} - z_0}{z_t - z_s} \qquad \text{(S9)}$$

By comparing eq (S9) with eq (2) of the main text, we arrive at the following expression of the parameter γ

$$\gamma = \frac{\delta\varepsilon_0(V)}{eV} = \frac{z_0 - z_{HOMO}}{z_t - z_s} \qquad \text{(S10)}$$

Notice that according to eq (S10) (which coincides with eq (5) in the main text), the bias-driven HOMO shift parameter γ is determined by the fractional HOMO offset from the junction's center (z_0 -z_{HOMO}) relative to junction's length (d=z_t -z_s).

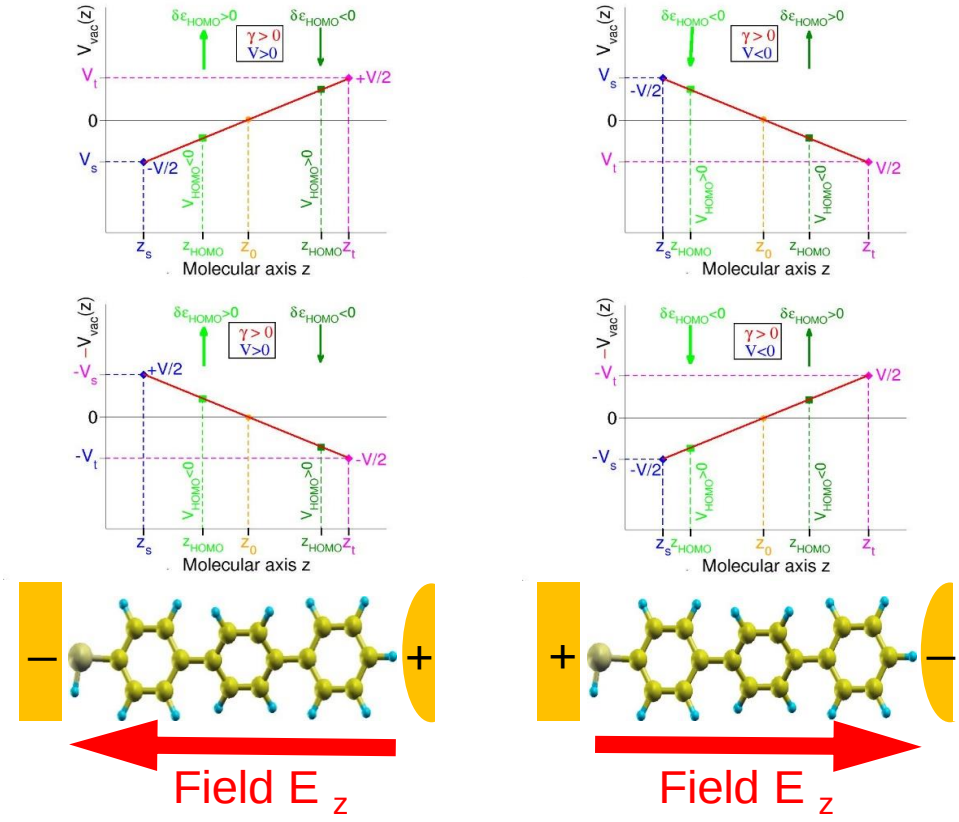

Figure S3. Schematic representation of the potentiometric rule to facilitate understanding the derivation of eqs S9 and S10. The various panels depict bias driven HOMO level shift expressed by eqs (S9) and (S10). Notice that the shift direction is determined both by the sign of V and by the (left-to-center or right-to-center) HOMO location. Reversing the sign of V on the Oy axis facilitates visualizing that HOMO shifts are in accord with potentiometer rule scenario.

Certainly, the above result is based on important simlifications: a point-like HOMO and a smooth, linear potential profile across the junction. Still, the idea underlying eq (S10) can easily be generalized to a realistic case. In cases of a HOMO possessing an extended spatial distribution $\rho_{HOMO}(x,y,z)=|\Psi_{HOMO}(x,y,z)|^2$ and an arbitrary potential profile $V(x,y,z)$, a general counterpart of eq (S9) can be expressed within the first order of perturbation theory (which we have validated against our transport measurements, see last paragraph of Section "Results")

$$\delta\varepsilon_0(V) = e\,\gamma V = -e\frac{\int dxdydz\rho_{HOMO}(x,y,z)v(x,y,z)}{\int dxdydz\rho_{HOMO}(x,y,z)} \qquad \text{(S11)}$$

As just said, eq (S11) (which coincides with eq (10) in the main text) is a result valid in the first order with respect to the external perturbation (=applied bias). Therefore, it is worth emphasizing that our experimental transport data do validate this approach: within experimental accuracy, we can rule out nonlinear (i.e. quadratic or cubic) contributions in V (denoted by γ_2, γ_3,... in the main text) in the RHS of eq (2) of the main text.

Results for $\delta\varepsilon_0(V)$ and $\gamma=\delta\varepsilon_0(V)/(eV)$ obtained from our quantum chemical calculations based on eq (S11) using the position dependent $\rho_{HOMO}(x,y,z)$ and $V(x,y,z)$ quantites computed microscopically are depicted by the red symbols in Figures 7A and 8B of the main text.

Important physical insight can be gained by examining the case of a potential profile whose spatial dependence in transverse directions can be disregarded, i.e., $v(z)\approx V(x,y,z)$. More precisely, we utilize a potential v(z) along the HOMO averaged over the transverse (x and y) spatial coordinates

$$v(z) = -e\frac{\int dxdy\rho_{HOMO}(x,y,z)v(x,y,z)}{\int dxdy\rho_{HOMO}(x,y,z)} \qquad \text{(S12)}$$

This is precisely what we expect for our CP-AFM OPTn junctions consisting of a bundle of molecules (ref. 3) contacted to polycrystalline electrodes, which inherently implies an averaging in transverse directions. In this case, eq (S11) reduces to

$$\delta\varepsilon_0(V) = e\,\gamma V = -e\frac{\int dz \rho_{HOMO}(z) v(z)}{\int dz \rho_{HOMO}(z)}, \rho_{HOMO}(z) \equiv \int dxdy\, \rho_{HOMO}(x,y,z) \qquad \text{(S13)}$$

where $\rho_{HOMO}(z)$ is the one-dimensional HOMO density projected along the transport direction z.

Noteworthily, the potential profile v(z) along the molecular axis z expressed by eq (S12) is a *HOMO-dedicated* average. This is exactly the potential that directly describes the bias-driven HOMO shift. The very detailed information depicted in Figures S5, S6 and S8 is motivated by the paramount importance of this quantity for the present analysis.

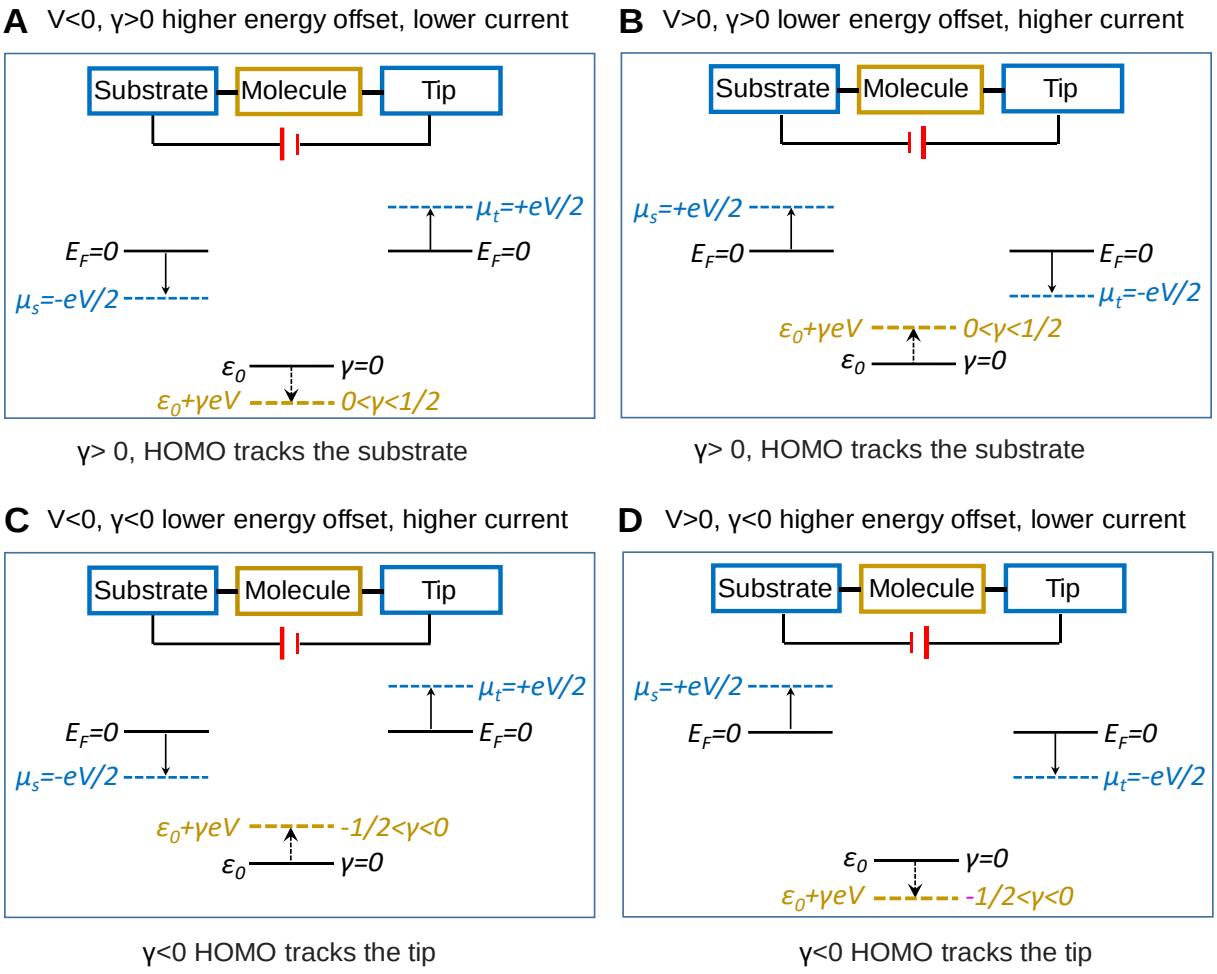

Figure S4. In cases where the potentiometer rule applies, the HOMO tracks the Fermi energy of the spatially closer electrode.

Additional Results of Quantum Chemical Calculations

Results for the Microscopic Potential Profile.

Although mathematically remarkable, the aforementioned agreement of the calculated γ_{theor} value with γ_{expt}, does not yet unravel the microscopic reason why the above estimate based on eq (5) is too large. More physical insight can be gained by examining the potential profile along molecular axis. Results of quantum chemical calculations for the (screened) potential *v(z)* along the line joining the end S and C atoms computed at fixed values of the applied (unscreened) field E_z are presented in Figures 7, S5, and S6. Noteworthily, the curves for *v(z)* calculated microscopically scale nearly perfectly with $E_z \equiv E_{ext}$ (Figure S5B). Figure S5C unravels another interesting aspect. Reversing applied bias polarity does not notably change the shape of the microscopic potential *v(z)*. That is, current rectification does not arise because the shape of the microscopic potential changes upon bias polarity reversal. This aspect is also important: in view of OPTn chemical asymmetry, this possibility cannot be ruled out a priori.

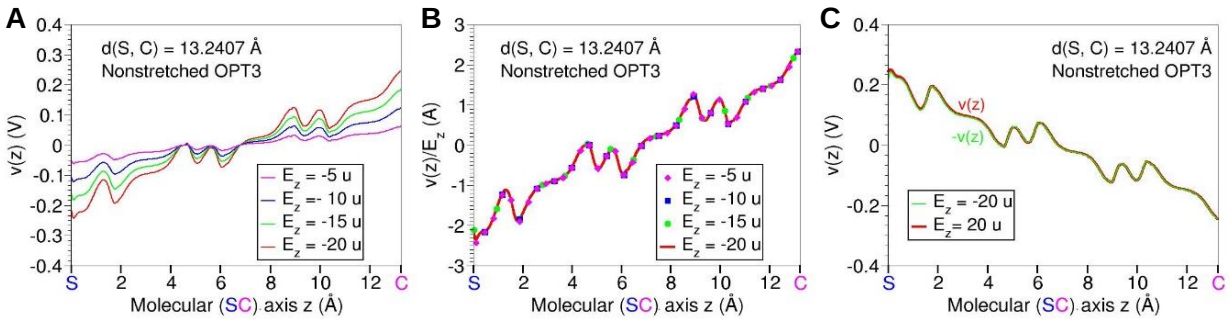

Figure S5. (A) Curves obtained from quantum chemical calculations for the microscopic potential *v(z)* along the line joining the end S and C atoms of OPT3 molecules placed in various external fields E_z. (B) The curves of A divided by the corresponding values of E_z. show that the microscopic potential *v(z)* is proportional to E_z. (C) Curves for *v(z)* illustrating that reversal of the applied electric field direction does not affect the shape of the microscopic potential. Given the OPT3 chemical asymmetry along the molecular axis z, this is a nontrivial property from the point of view of current rectification. Field intensities E_z in inset expressed in GAUSSIAN units ($u = 10^{-4}$ *a.u.* = *0.0514* V/nm) to facilitate the preparation of the input files for quantum chemical calculations (E_z = *-5* u = *-0.257* V/nm, E_z = *-10* u = *-0.514* V/nm, E_z = *-15* u = *-0.771* V/nm, E_z = *-20* u = *-1.028* V/nm).

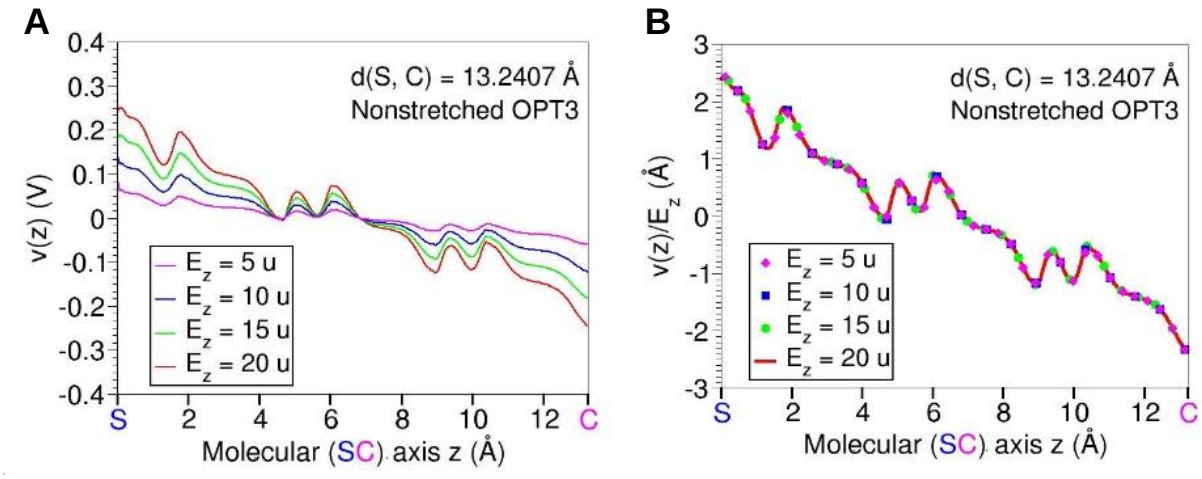

Figure S6. Same as in Figure S5A and S5B but for negative bias (V<0). Field intensities E_z in inset expressed in GAUSSIAN units ($u = 10^{-4}$ *a.u.* = *0.0514* V/nm) to facilitate the preparation of the input files for quantum chemical calculations (E_z = *5* u = *0.257* V/nm, E_z = *10* u = *0.514* V/nm, E_z = *15* u = *0.771* V/nm, E_z = *20* u = *1.028* V/nm).

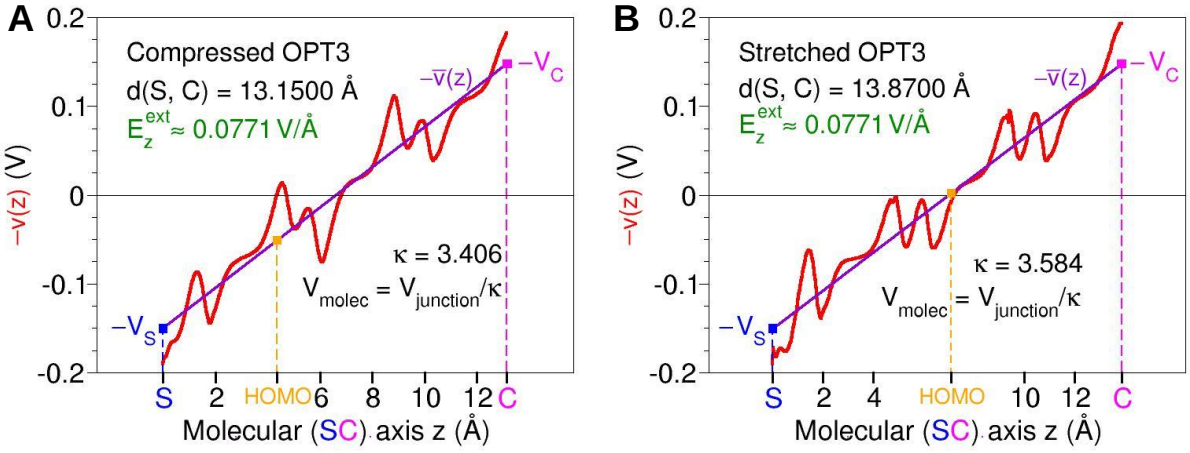

Figure S7. Same as in Figure 7B of the main text but for: (A) compressed OPT3 and (B) stretched OPT3.

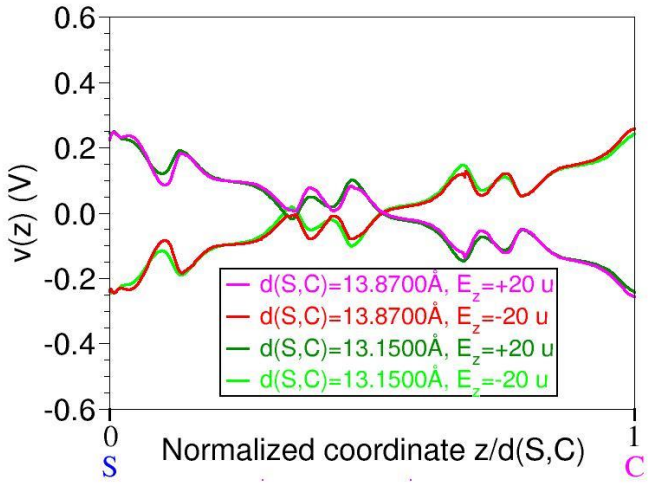

Figure S8. Results of quantum chemical calculations revealing that OPT3 mechanical deformation has little impact on the shape of the microscopic potential. Notice the normalized coordinate on the abscissa, which makes the coordinates of the end S and C atoms (0 and 1, respectively) independent of molecule's elongation. External electric field expressed in GAUSSIAN unit u=10^{-4} a.u. = 0.0514 volt/nm (E_z = ±*20* u = ±*1.028* V/nm).

Embedded OPTn Molecules versus Isolated OPTn Molecules.

Although molecules embedded in junctions may in general have properties significantly different from isolated molecules, in some cases coupling to electrodes may not too strongly affect certain properties. This could be expected especially in case of sufficiently long species. This was an important reason why here we focused on OPT3, which is the longest (commercially) available OPTn or at least at our disposal.

What we used in the calculations based on eqs (5) to (11) is the HOMO spatial density of the isolated OPT3 molecule delimited by the transverse planes through the S and C atoms at the two molecular ends. It is the fact that our theoretical values for γ agree well with the experimental

ones that ultimately demonstrates that, indeed, the HOMO of the embedded molecules does not substantially penetrate into electrodes. Still, a microscopic justification of this behavior would be desirable. To this aim, we have computed HOMO's longitudinal extension around its center of charge $z_{HOMO} \equiv \langle z \rangle$. Amounting to $\sqrt{\langle z^2 \rangle - \langle z \rangle^2} = 3.89$ Å, it is smaller than HOMO's distance z_{HOMO}-z_S=4.46 Å and z_C-z_{HOMO}=8.78 Å to the end S and C atoms, respectively. These values make it clear why in our present quantitative analysis corrections to OPT3's HOMO due to electrodes could safely be neglected. This is an obvious simplification also for another important reason. In the present study, as the case of most experimental platforms to fabricate molecular junctions, we employed polycrystalline electrodes. This is an important, albeit ubiquitously overlooked challenge for theory, which often compares estimates computed for molecules adsorbed, e.g. on (111) FCC gold with data measured with polycrystalline gold electrodes. What is highly problematic here is that differences in properties of molecules adsorbed at different adsorption sites can be as substantial as differences between embedded and isolated molecules. Parenthetically one could also note at this point that HOMO's extension in transverse direction ($\sqrt{\langle x^2 \rangle - \langle x \rangle^2} = 0.79$ Å and $\sqrt{\langle y^2 \rangle - \langle y \rangle^2} = 0.82$ Å) is much smaller than the average interchain spacing 5.35 Å. The latter corresponds to a coverage $\Sigma \approx 3.5$ molecules/nm^2, the value we have obtained for our SAMs via Rutherford backscattering (RBS) and nuclear reaction analysis (NRA).[4] This remark is important because it gives further support to conclusions of our earlier reports (e.g. refs. 5,6) that charge transport through our OPTn CP-AFM junctions is genuinely one dimensional, i.e. occurs along individual molecules without significant "perturbations" of interchain electron tunneling.

Relationship between Molecule's and Junction's Elongations

To obtain the (one-to-one!) correspondence between $\Delta d(\mathrm{S,C}) = d(\mathrm{S,C}) - d_{equil}(\mathrm{S,C})$ and $\Delta d_{junction}$ =

$L - L_{equil}$ (the quantities on the Ox-axis in Figure 8B) we proceed as follows. We perform geometry optimization at fixed C-S distances *d(S,C)* smaller/larger than the equilibrium value ($d_{equil}(S,C) = 13.2407$ Å for OPT3) and determine the force F_{molec} = f(*d(S,C)*) (compressive force $F_{molec} > 0$, tensile force $F_{molec} < 0$, respectively). With this force per molecule F_{molec} in hand, we have an equation relating the force per junction F (applied in experiment) and the contact radius a: $F = F_{molec}\, N = F_{molec}\, \Sigma\, \pi\, a^2$ (N being the number of molecules per junction and Σ the experimentally available SAM coverage[4]). Along with two other equations of the MD model (these are equations S7 and S8 in ref. 7) we thus have a system of three transcendent algebraic equations, whose numerical solution determines the values of the three unknown quantities F, a, and m (see ref. 7 for details on the quantity m) as a function of F_{molec} = f(*d(S,C)*). Once at given *d(*S,C*) a* and *m* are known, we compute the corresponding indentation *h* using the third equation of the MD model (this is equation S9 in ref. 7). Junction's elongation ($\Delta d_{junction} = L - L_{equil}$) is related straightforwardly related to the indentation: with MD's convention sign $\Delta d_{junction} = h_{equil} - h$. Throughout, the subscript label *equil* refers to the equilibrium geometry of the nonstretched molecule ($d_{equil}(S,C) = 13.2407$ Å at $F_{molec,\, equil} = 0$). Needless to say, $\Delta d_{junction} - \Delta d$(S,C) represents the contacts' elongation, which is obviously accounted for within the MD model. At pull-off, out of the total junction's elongation of $\Delta d_{junction} = 0.84$ Å, Δd(S,C) = 0.63 Å is the molecule's elongation; the difference of $0.84 - 0.63 = 0.21$ Å should basically be the elongation of the weaker van der Waals bond. Noteworthily, from the measured pull-off force, the MD model allows us to compute the work of adhesion (denoted by γ in ref. 7, but obviously having nothing to do with the present quantity γ), which contains just the information on our real junctions with polycrystalline electrodes (and hence inherently inaccessible via contacts' microscopic modeling) we need to estimate junction's length/elongation under stretching.

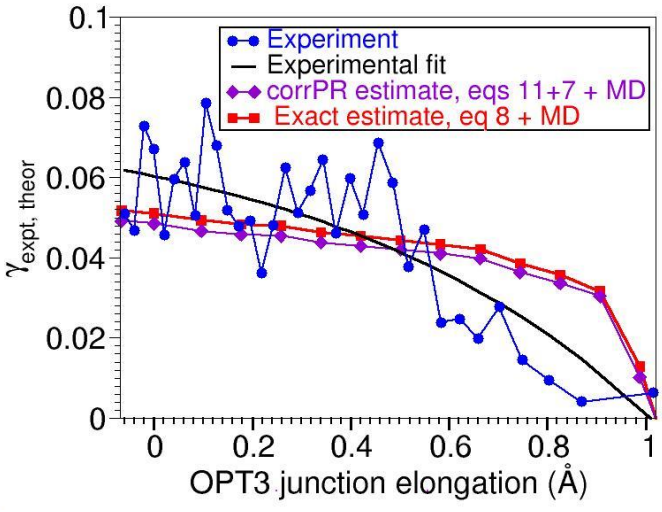

Figure S9. Comparison of the experimental and theoretical γ. The theoretical values of γ were obtained by means of quantum chemical calculations using equations indicated in the inset. The relationship between molecule's and junction's elongation used to obtain the theoretical curves was deduced by combining quantum chemical calculations with Maugis-Dugdale model, as explained in SI's last section. As visible, the theoretical values quantitatively agree with those deduced from the experimental data.

References:

1 C. Caroli, R. Combescot, P. Nozieres and D. Saint-James, *J. Phys. C Solid State Phys.*, 1971, **4**, 916–929.

2 H. Haug and A.-P. Jauho, *Quantum Kinetics in Transport and Optics of Semiconductors*, Springer-Verlag Berlin Heidelberg, Berlin Heidelberg New York, 2nd edn., 2008.

3 Z. Xie, I. Bâldea and C. D. Frisbie, *J. Am. Chem. Soc.*, 2019, **141**, 3670–3681.

4 A. T. Demissie, G. Haugstad and C. D. Frisbie, *J. Phys. Chem. Lett.*, 2016, **7**, 3477–3481.

5 I. Bâldea, Z. Xie and C. D. Frisbie, *Nanoscale*, 2015, **7**, 10465–10471.

6 Z. Xie, I. Bâldea, C. E. Smith, Y. Wu and C. D. Frisbie, *ACS Nano*, 2015, **9**, 8022–8036.

7 Z. Xie, I. Bâldea, A. T. Demissie, C. E. Smith, Y. Wu, G. Haugstad and C. D. Frisbie, *J. Am. Chem. Soc.*, 2017, **139**, 5696–5699.